CAUCHY – Jurnal Matematika Murni dan Aplikasi
Volume 11 (2) (2026), Pages 2008–2025
p-ISSN: 2086-0382; e-ISSN: 2477-3344

# Neimark–Sacker Bifurcation in a Discrete Host–Parasitoid System with Host Refuge Mechanism

Ardianto Ramadhan and Abadi*

*Department of Mathematics, Faculty of Mathematics and Natural Sciences, Universitas Negeri Surabaya, Indonesia*

**Abstract**

This study investigates the local dynamics of a discrete-time host–parasitoid model incorporating a proportional host refuge mechanism. The objective is to clarify how host growth and refuge fraction govern the transitions among extinction, stable coexistence, and oscillatory dynamics. Linearization, stability conditions, discriminant analysis, and local normal-form calculations are used to determine the existence and stability of the extinction and coexistence fixed points and to characterize their local behavior. The boundary between extinction and coexistence is identified as a nonhyperbolic threshold supporting a continuum of boundary fixed points. Within the stable coexistence region, the discriminant separates node-type convergence from damped spiral convergence. Variation in the refuge fraction is shown to induce a supercritical Neimark–Sacker bifurcation, producing a stable invariant closed curve and bounded oscillations on the weak-refuge side near the critical threshold. Numerical phase portraits, time series, bifurcation diagrams, and a two-parameter map support the analytical findings. These results provide a unified description of extinction, stable coexistence, and oscillatory behavior in the refuge model.

**Keywords:** Host–Parasitoid Model; Discrete Dynamical System; Invariant Closed Curve; Neimark–Sacker Bifurcation; Proportional Refuge



## 1. Introduction

Discrete mathematical models describe systems that evolve through distinct time intervals and are useful across various fields, including fast-food consumption [1] and information diffusion [2]. In ecology, discrete-time formulations have been used to investigate predator–prey interactions and other population processes governed by generation-to-generation updates [3–5]. Such a framework is particularly appropriate for host–parasitoid interactions involving insects, because many species have seasonal life cycles with synchronized and non-overlapping generations.

The Nicholson–Bailey model is a classical discrete-time framework for describing host–parasitoid interactions across successive generations [6]. Although the model provides a simple representation of host reproduction and parasitoid attack through an escape probability, the coexistence fixed point can be unstable under the original assumptions. This limitation has motivated modified discrete host–parasitoid models involving alternative functional responses, host growth functions, and threshold mechanisms [7–9].

*Corresponding author. E-mail: abadi@unesa.ac.id

Received: July 15, 2026 Revised: August 15, 2026 Accepted: September 1, 2026
DOI: https://doi.org/10.18860/cauchy.v11i2.45034

One biologically relevant extension is the refuge mechanism, in which a portion of the host population is protected from parasitoid attack because of habitat structure, behavior, or limited accessibility [10, 11]. A spatial refuge is one example of this mechanism. The searching efficiency of the pupal parasitoid *Dirhinus giffardii* against the oriental fruit fly *Bactrocera dorsalis* is affected by the age of host pupae and their depth within plant debris [12]. Mathematical studies have shown that refuge mechanisms can alter the existence and local stability of fixed points and can substantially change the long-term behavior of host–parasitoid systems [13, 14].

The qualitative study of discrete ecological models commonly begins with the existence and local stability of fixed points, followed by bifurcation analysis when parameter variation changes the local dynamics. Neimark–Sacker bifurcation has been used to explain the onset of sustained oscillations in discrete predator–prey and related ecological models [15–17], while related analyses have examined invariant closed curves and bifurcation phenomena in host–parasitoid and other discrete population models [18–20]. Among these studies, Bešo et al. [18] considered refuge-based host–parasitoid models with Beverton–Holt density regulation and a general escape function. They derived coexistence stability conditions and Neimark–Sacker bifurcation criteria for this density-regulated class. Thus, Neimark–Sacker bifurcation is already known in refuge-based host–parasitoid models, but under assumptions that differ from the no-self-limitation setting considered here.

Among the formulations studied by Singh [21], the proportional-refuge Nicholson–Bailey model without intrinsic host self-limitation corresponds to the system analyzed here. Singh identified the coexistence fixed point and its stability threshold, with locally stable coexistence for $\mu^* < \mu < \frac{1}{r}$, bounded oscillations under weaker refuge, and unbounded growth for refuge levels above $\frac{1}{r}$. Therefore, the coexistence stability condition is not claimed as new. The present analysis instead refines the stable region by distinguishing node-type from damped spiral convergence, characterizes the fixed-point structure at the extinction–coexistence boundary, and determines how $E_1$ loses stability at the critical refuge value. The main result establishes a supercritical Neimark–Sacker bifurcation, with a stable invariant closed curve emerging locally on the weak-refuge side of the threshold. Numerical simulations and a two-parameter map illustrate these analytical results.

## 2. Methods

The mathematical formulation considered in this study, together with the theoretical framework required for its analysis, is presented in the following subsection.

### 2.1. Mathematical Model Formulation

The discrete-time host–parasitoid system analyzed in this paper is the proportional-refuge Nicholson–Bailey formulation considered by Singh [21] in the absence of intrinsic host self-limitation. Accordingly, no carrying-capacity term is included in the host growth process. Let $H_t$ and $P_t$ denote the host and parasitoid population densities, respectively, at generation $t = 0, 1, 2, \ldots$.

In the absence of parasitism, the host population reproduces with intrinsic reproduction rate $r$. The host–parasitoid interaction is represented by the escape function $S(P_t) = \mu + (1-\mu)e^{-cP_t}$, which gives the fraction of hosts escaping parasitism. Here, $\mu$ is the protected host fraction, while $e^{-cP_t}$ is the escape probability under the random-search assumption, with $c$ denoting the parasitoid search efficiency or attack rate. The model is therefore given by

$$\begin{aligned} H_{t+1} &= rH_tS(P_t) \\ P_{t+1} &= krH_t(1 - S(P_t)) \end{aligned} \tag{1}$$

The parameter $k$ denotes the average number of new parasitoids emerging from one parasitized host. The first equation describes the host population surviving parasitism, while the second

describes parasitoid production from parasitized hosts. Throughout this paper, the biologically admissible parameter region is $r > 0$, $k \geq 1$, $c > 0$, $0 \leq \mu < 1$, with nonnegative initial conditions. Since $0 < S(P_t) \leq 1$ for all $P_t \geq 0$, system (1) maps the nonnegative state space into itself, and every nonnegative initial condition generates a nonnegative solution.

## 2.2. Review of Stability Analysis Theory

**Definition 1.** [22] A steady-state fixed point of the nonlinear system of difference equations $x_{t+1} = \phi(x_t)$ is a vector $\bar{x} \in \mathbb{R}^n$ such that $\bar{x} = \phi(\bar{x})$.

Referring to Galor [22], the local behavior around a fixed point is analyzed using linearization. Let $y_t = x_t - \bar{x}$. The local dynamics are determined by $y_{t+1} = Jy_t$, where $J$ is the Jacobian matrix evaluated at the fixed point. Since system (1) is two-dimensional, $J$ is a $2 \times 2$ matrix, and local stability is determined by the moduli of its eigenvalues.

**Definition 2.** [22] Consider the map $\phi : \mathbb{R}^n \to \mathbb{R}^n$ and let $\mathcal{D}\phi(\bar{x})$ be the Jacobian matrix of $\phi(x)$ evaluated at a fixed point $\bar{x}$. The fixed point $\bar{x}$ is called a hyperbolic fixed point if $\mathcal{D}\phi(\bar{x})$ has no eigenvalues of modulus one.

If at least one eigenvalue of $J$ lies on the unit circle, the corresponding fixed point is nonhyperbolic by Definition 2 and requires separate local analysis. The eigenvalues $\lambda$ of $J$ are determined from $\det(J - \lambda I) = 0$. In this study, the characteristic equation yields

$$\lambda^2 - \tau\lambda + \Delta = 0 \tag{2}$$

where $\tau = \operatorname{tr}(J)$ is the trace and $\Delta = \det(J)$ is the determinant of the matrix $J$.

**Theorem 1.** *[23] Let $J$ be a $2 \times 2$ matrix. Then $|\lambda_{1,2}| < 1$ if and only if $|\tau| - 1 < \Delta < 1$.*

**Corollary 1.** *[23] A fixed point is asymptotically stable if the Jacobian matrix $J$ evaluated at the fixed point satisfies the stability condition in Theorem 1, which is equivalent to the following three stability bounds:* (1) $1 - \tau + \Delta > 0$, (2) $1 + \tau + \Delta > 0$, (3) $\Delta < 1$.

**Theorem 2.** *[23] The following statements hold for any $2 \times 2$ matrix $J$.*

1. *If $1 - \tau + \Delta = 0$, then the eigenvalues of $J$ are $\lambda_1 = 1$ and $\lambda_2 = \Delta$.*
2. *If $1 + \tau + \Delta = 0$, then the eigenvalues of $J$ are $\lambda_1 = -1$ and $\lambda_2 = -\Delta$.*
3. *If $|\tau| < 2$ and $\Delta = 1$, then the eigenvalues of $J$ are $e^{\pm i\theta}$, where $\theta = \cos^{-1}\left(\frac{\tau}{2}\right)$.*

From the characteristic equation (2), the discriminant is defined by

$$D = \tau^2 - 4\Delta \tag{3}$$

The sign of $D$ determines the local eigenvalue types and the convergence behavior within the stable region. If $D > 0$, the eigenvalues are real and distinct, whereas $D = 0$ gives repeated real eigenvalues. Thus, $D \geq 0$ corresponds to real eigenvalues and node-type convergence within the stable region. If $D < 0$, the eigenvalues form a complex conjugate pair,

$$\lambda_{1,2} = \alpha \pm i\beta \tag{4}$$

where $\alpha, \beta \in \mathbb{R}$ and $\beta \neq 0$, corresponding to spiral-type convergence with damped oscillations within the stable region. When these eigenvalues lie on the unit circle, Theorem 2 gives $\lambda_{1,2} = e^{\pm i\theta}$. By Euler's formula, this form is equivalent to (4), with $\alpha = \cos\theta$ and $\beta = \sin\theta$.

## 3. Results and Discussion

The dynamical behavior of the system is examined by first considering the existence and characterization of its fixed points.

### 3.1. Existence of Fixed Points

**Proposition 1.** *The host–parasitoid system (1) admits the trivial fixed point $E_0 = (0, 0)$, representing population extinction, which always exists for all admissible parameter values. The nontrivial fixed point $E_1 = (\bar{H}, \bar{P})$, representing host–parasitoid coexistence, is given by*

$$\bar{H} = \frac{L}{kc(r-1)}, \quad \bar{P} = \frac{L}{c}$$

*where $L = \ln\left(\frac{r(1-\mu)}{1-r\mu}\right)$. This fixed point exists and both population densities are positive if the parameter conditions $r > 1$ and $0 \leq \mu < \frac{1}{r}$ are satisfied.*

*Proof.* At a fixed point, the first equation gives $\bar{H} = 0$ or $rS(\bar{P}) = 1$. The first possibility yields the extinction fixed point $E_0 = (0, 0)$. For a coexistence fixed point, $S(\bar{P}) = \frac{1}{r}$, which gives $\bar{P} = \frac{\ln\left(\frac{r(1-\mu)}{1-r\mu}\right)}{c}$. The second fixed-point equation gives $\bar{P} = k(r-1)\bar{H}$. Let $L = \ln\left(\frac{r(1-\mu)}{1-r\mu}\right)$. Then, $\bar{H} = \frac{L}{kc(r-1)}$ and $\bar{P} = \frac{L}{c}$. For $0 \leq \mu < 1$, the numerator $r(1-\mu)$ in $L$ is positive. Therefore, $L$ is real only when $1 - r\mu > 0$, which gives $\mu < \frac{1}{r}$. Under this condition, $\frac{r(1-\mu)}{1-r\mu} > 1$ if $r > 1$. Hence, $L > 0$, and consequently $\bar{P} > 0$ and $\bar{H} > 0$ precisely when $r > 1$ and $0 \leq \mu < \frac{1}{r}$. Therefore, the coexistence fixed point exists under the stated conditions. □

### 3.2. Stability Analysis of Fixed Points

**Theorem 3.** *The trivial fixed point $E_0 = (0, 0)$ is locally asymptotically stable if and only if $0 < r < 1$. In this parameter range, $E_0$ is a stable node.*

*Proof.* Evaluating the Jacobian matrix at the fixed point $E_0 = (0, 0)$ gives

$$J = \begin{pmatrix} r\left(\mu + (1-\mu)e^{-c\bar{P}}\right) & -cr\bar{H}\,(1-\mu)\,e^{-c\bar{P}} \\ kr\,(1-\mu)\left(1 - e^{-c\bar{P}}\right) & ckr\bar{H}\,(1-\mu)\,e^{-c\bar{P}} \end{pmatrix}\Bigg|_{(0,0)} = \begin{pmatrix} r & 0 \\ 0 & 0 \end{pmatrix}$$

Thus $\tau = r$ and $\Delta = 0$. By Corollary 1, local asymptotic stability is determined by three inequalities. The first inequality gives $r < 1$, while the other two hold since $r > 0$ and $\Delta = 0$. Hence, $E_0$ is locally asymptotically stable if and only if $0 < r < 1$. For the local eigenvalue classification, equation (3) gives $D = r^2 > 0$. Therefore, the eigenvalues are real and distinct. In the stability region, this corresponds to node-type convergence, so $E_0$ is a stable node. □

**Theorem 4.** *Based on Proposition 1, assume $r > 1$ and $0 \leq \mu < \frac{1}{r}$ so that the nontrivial fixed point $E_1 = \left(\bar{H}, \bar{P}\right)$ exists. With $L = \ln\left(\frac{r(1-\mu)}{1-r\mu}\right)$, the coexistence fixed point $E_1 =$*

$\left(\bar{H}, \bar{P}\right)$ *is locally asymptotically stable if and only if*

$$\frac{rL\,(1-r\mu)}{r-1} < 1 \tag{5}$$

*Proof.* Evaluating the Jacobian matrix at the fixed point $E_1 = (\bar{H}, \bar{P})$ in Proposition 1 yields

$$J = \begin{pmatrix} r\left(\mu + (1-\mu)e^{-c\bar{P}}\right) & -cr\bar{H}\,(1-\mu)\,e^{-c\bar{P}} \\ kr\,(1-\mu)\left(1-e^{-c\bar{P}}\right) & ckr\bar{H}\,(1-\mu)\,e^{-c\bar{P}} \end{pmatrix}\Bigg|_{(\bar{H},\bar{P})} = \begin{pmatrix} 1 & -\frac{(1-r\mu)L}{k(r-1)} \\ k\,(r-1) & \frac{(1-r\mu)L}{r-1} \end{pmatrix}$$

with $\bar{H}$ as given in Proposition 1. Thus, the trace and determinant are

$$\tau = 1 + \frac{(1-r\mu)\,L}{r-1} \quad \text{and} \quad \Delta = \frac{rL\,(1-r\mu)}{r-1} \tag{6}$$

which imply the relation

$$\tau = 1 + \frac{\Delta}{r} \tag{7}$$

By Corollary 1, the local asymptotic stability of $E_1$ is determined by the three stability inequalities. Since $r > 1$ and $0 \le \mu < \frac{1}{r}$, it follows that $L > 0$, $1 - r\mu > 0$, and $\Delta > 0$. Using (7), the first two stability bounds are automatically satisfied. Therefore, the remaining condition $\Delta < 1$, equivalently (5), is necessary and sufficient for the local asymptotic stability of $E_1$. □

The local classification of $E_1$ within the stable region can be further refined using the discriminant, as stated in the following theorem.

**Theorem 5.** *Assume that the coexistence fixed point $E_1$ exists and is locally asymptotically stable as stated in Theorem 4. Then the local classification of the stable coexistence fixed point $E_1$ is determined by the oscillation threshold*

$$\Delta_{\text{osc}} = 2r^2 - r - 2r\sqrt{r(r-1)} \tag{8}$$

*with the following local classification:*

1. *If $0 < \Delta < \Delta_{\text{osc}}$, $D > 0$, so the eigenvalues are real and $E_1$ is a stable node.*
2. *If $\Delta_{\text{osc}} < \Delta < 1$, $D < 0$, so the eigenvalues are complex conjugates and $E_1$ is a spiral sink.*
3. *If $\Delta = \Delta_{\text{osc}}$, $D = 0$, so the repeated real eigenvalue yields non-oscillatory convergence.*

*Proof.* Within the stability region $0 < \Delta < 1$, the local classification of $E_1$ is determined by the sign of $D$. Using (7), equation (3) becomes $D(\Delta) = \psi(\Delta)/r^2$, where $\psi(\Delta) = \Delta^2 + (2r - 4r^2)\Delta + r^2$. Since $r > 1$, $D(\Delta)$ and $\psi(\Delta)$ have the same sign. Solving $\psi(\Delta) = 0$ gives

$$\Delta_{1,2} = r\,(2r-1) \pm 2r\sqrt{r\,(r-1)}.$$

Of these roots, only $\Delta_{\text{osc}}$ defined in (8) lies in $0 < \Delta < 1$, while the other lies outside the stability interval. Since $\psi$ is an upward-opening quadratic, $\psi(\Delta) > 0$ for $0 < \Delta < \Delta_{\text{osc}}$,

$\psi(\Delta) = 0$ at $\Delta = \Delta_{\text{osc}}$, and $\psi(\Delta) < 0$ for $\Delta_{\text{osc}} < \Delta < 1$. Accordingly, these sign cases establish the eigenvalue and local stability classifications stated in the theorem. □

### 3.3. Dynamics Near the Extinction Threshold

The coexistence fixed point $E_1$ exists only for $r > 1$. Therefore, the boundary case $r = 1$ is considered separately by examining the extinction fixed point $E_0$ and the corresponding fixed-point equations. This analysis characterizes the fixed-point structure at the boundary between extinction and coexistence. At $r = 1$, the Jacobian at $E_0$ has $\tau = 1$ and $\Delta = 0$, so $1 - \tau + \Delta = 0$. By Theorem 2, its eigenvalues are $\lambda_1 = 1$ and $\lambda_2 = 0$; hence, $E_0$ is nonhyperbolic by Definition 2.

Since $r = 1$, the fixed-point equations reduce to $\bar{H} = \bar{H}S(\bar{P})$ and $\bar{P} = k\bar{H}\left(1 - S(\bar{P})\right)$. If $\bar{H} = 0$, then $\bar{P} = 0$, yielding $E_0$. If $\bar{H} > 0$, the first equation requires $S(\bar{P}) = 1$, which for $0 \le \mu < 1$ implies $\bar{P} = 0$. Thus, the system admits the continuum of boundary fixed points $\{(\bar{H}, 0) \mid \bar{H} \ge 0\}$. Local asymptotic stability requires an isolated fixed point [22]. Since every neighborhood of $E_0$ contains another fixed point $(\bar{H}, 0)$ whose trajectory remains stationary, $E_0$ is not locally asymptotically stable at $r = 1$. Therefore, $r = 1$ is a nonhyperbolic extinction threshold rather than a classical transcritical bifurcation, as it produces a continuum of boundary fixed points instead of an intersection of two isolated fixed-point branches.

### 3.4. Neimark–Sacker Bifurcation Analysis

From Theorem 4, the local stability of $E_1$ is governed by the condition $\Delta < 1$. Thus, a loss of stability may occur at $\Delta = 1$, where the complex-conjugate eigenvalues may reach the unit circle.

**Lemma 1.** *[24] The appearance of a topologically nonequivalent phase portrait under variation of parameters is called a bifurcation.*

**Lemma 2.** *[24] The bifurcation corresponding to the presence of $\lambda_{1,2} = e^{\pm i\theta_0}$, $0 < \theta_0 < \pi$, is called a Neimark–Sacker bifurcation.*

Before verifying the Neimark–Sacker conditions, it is necessary to establish that, for every $r > 1$, the equation $\Delta(\mu) = 1$ has exactly one admissible critical value $\mu^*$, as shown in the following proposition.

**Proposition 2.** *Assume $r > 1$ and $0 \le \mu < \frac{1}{r}$. Let $\Delta(\mu)$ be the determinant of the Jacobian matrix at $E_1$ given in (6). Then $\Delta$ is continuous on $[0, \frac{1}{r})$, with $\Delta(0) > 1$ and $\lim_{\mu \to (\frac{1}{r})^-} \Delta(\mu) = 0$. Moreover, $\Delta'(\mu) < 0$ for $0 < \mu < \frac{1}{r}$, so $\Delta$ is strictly decreasing on $[0, \frac{1}{r})$. Consequently, for every $r > 1$, there exists a unique critical refuge value $\mu^* \in (0, \frac{1}{r})$ such that $\Delta(\mu^*) = 1$.*

*Proof.* For $0 \le \mu < \frac{1}{r}$, $1 - r\mu > 0$ and $1 - \mu > 0$. Hence, the logarithmic term in $\Delta(\mu)$ is well-defined and continuous, so $\Delta$ is continuous on $[0, \frac{1}{r})$. Let $q = 1 - r\mu$. Then $0 < q \le 1$ and $r(1 - \mu) = r - 1 + q$, so

$$\Delta(\mu) = \frac{rq}{r-1} \ln\left(\frac{r-1+q}{q}\right).$$

At $\mu = 0$, $q = 1$ and $\Delta(0) = \frac{r \ln r}{r-1}$. Consider $g(z) = z \ln z - z + 1$ for $z \ge 1$. Since $g(1) = 0$ and $g'(z) = \ln z > 0$ for $z > 1$, it follows that $g(z) > 0$, equivalently $\ln z > 1 - \frac{1}{z}$ for $z > 1$. Taking $z = r > 1$ gives $\ln r > \frac{r-1}{r}$, and hence $\Delta(0) > 1$.
As $\mu \to (\frac{1}{r})^-$, $q \to 0^+$ and $\Delta(\mu) = \frac{r}{r-1}[q \ln(r - 1 + q) - q \ln q]$. Since $\ln(r-1+q) \to \ln(r-1)$,

it follows that $q\ln(r-1+q)\to 0$. Moreover, $-q\ln q=\frac{\ln(1/q)}{1/q}$, and L'Hôpital's rule gives $\lim_{q\to 0^+}\frac{\ln(1/q)}{1/q}=\lim_{q\to 0^+} q=0$. Therefore, $\lim_{\mu\to(\frac{1}{r})^-}\Delta(\mu)=0$.
To establish strict monotonicity, recall that $L=\ln\left(\frac{r(1-\mu)}{1-r\mu}\right)$. Differentiating gives $L'(\mu)=\frac{r-1}{(1-\mu)(1-r\mu)}$, and hence

$$\Delta'(\mu)=\frac{r^2}{r-1}\left[-L+\frac{r-1}{r(1-\mu)}\right].$$

For $0\le\mu<\frac{1}{r}$, $r(1-\mu)-(1-r\mu)=r-1>0$, so $\frac{r(1-\mu)}{1-r\mu}>1$. Applying the logarithmic inequality above with $z=\frac{r(1-\mu)}{1-r\mu}$ gives

$$L>1-\frac{1-r\mu}{r(1-\mu)}=\frac{r-1}{r(1-\mu)}.$$

Thus, $-L+\frac{r-1}{r(1-\mu)}<0$. Since $\frac{r^2}{r-1}>0$ for $r>1$, it follows that $\Delta'(\mu)<0$ for $0<\mu<\frac{1}{r}$, and therefore $\Delta$ is strictly decreasing on $[0,\frac{1}{r})$.
Finally, since $\Delta(0)>1$ and $\lim_{\mu\to(\frac{1}{r})^-}\Delta(\mu)=0$, $\Delta(\mu)<1$ for $\mu$ sufficiently close to $\frac{1}{r}$ from the left. By continuity, the Intermediate Value Theorem guarantees the existence of $\mu^*\in(0,\frac{1}{r})$ such that $\Delta(\mu^*)=1$. Since $\Delta$ is strictly decreasing on $[0,\frac{1}{r})$, this value is unique. □

**Theorem 6.** *Assume the coexistence fixed point $E_1$ exists as stated in Theorem 4. Let $\mu^*$ denote the unique critical refuge value given by Proposition 2, satisfying $\Delta(\mu^*)=1$, equivalently*

$$\frac{rL^*(1-r\mu^*)}{r-1}=1,\quad L^*=\ln\left(\frac{r(1-\mu^*)}{1-r\mu^*}\right) \tag{9}$$

*Then the trace and determinant of the Jacobian matrix at $E_1$ satisfy the third statement of Theorem 2. Consequently, at $\mu=\mu^*$, the eigenvalues satisfy the Neimark–Sacker condition in Lemma 2.*

*Proof.* The Jacobian determinant at $E_1$ is given by (6). Since $\Delta(\mu^*)=1$, relation (7) gives $\tau(\mu^*)=1+\frac{1}{r}$. Since $r>1$, $|\tau(\mu^*)|<2$; hence, the third statement of Theorem 2 is satisfied at $\mu=\mu^*$. The eigenvalues can therefore be written as $\lambda_{1,2}=e^{\pm i\theta}$, where $\theta=\cos^{-1}\left(\frac{\tau}{2}\right)$. At $\mu=\mu^*$, this gives $\theta_0=\theta(\mu^*)=\cos^{-1}\left(\frac{r+1}{2r}\right)$ and $\lambda_{1,2}=e^{\pm i\theta_0}$. Since $r>1$, $\frac{1}{2}<\frac{r+1}{2r}<1$, implying $0<\theta_0<\frac{\pi}{3}<\pi$. Thus, the Neimark–Sacker condition in Lemma 2 is satisfied. □

By Proposition 2 and Theorem 6, under the admissibility condition for $E_1$ in Theorem 4, the parameter values at which the coexistence fixed point reaches the Neimark–Sacker critical boundary form the set

$$\mathcal{H}_{\mathrm{NS}}=\left\{(r,k,c,\mu^*):r>1,\quad k\ge 1,\quad c>0,\quad 0<\mu^*<\frac{1}{r},\quad \frac{rL^*(1-r\mu^*)}{r-1}=1\right\}. \tag{10}$$

The Neimark–Sacker bifurcation analysis follows the bifurcation theory of Kuznetsov [24] and Guckenheimer–Holmes [25], as used in related discrete ecological models [15–18, 20]. The refuge fraction is chosen as the bifurcation parameter because it directly controls the protected host proportion. Let $\widetilde{\mu}$ be a small perturbation such that $\mu=\mu^*+\widetilde{\mu}$, where $|\widetilde{\mu}|\ll 1$. Thus, $\widetilde{\mu}=0$ corresponds to the critical value $\mu=\mu^*$. Define $L(\widetilde{\mu})=\ln\left(\frac{r(1-\mu^*-\widetilde{\mu})}{1-r(\mu^*+\widetilde{\mu})}\right)$. Then, the trace and

determinant of the Jacobian matrix at the perturbed coexistence fixed point are

$$\tau(\widetilde{\mu}) = 1 + \frac{(1 - r(\mu^* + \widetilde{\mu}))L(\widetilde{\mu})}{r-1} \quad \text{and} \quad \Delta(\widetilde{\mu}) = \frac{r(1 - r(\mu^* + \widetilde{\mu}))L(\widetilde{\mu})}{r-1}$$

At zero perturbation, $\widetilde{\mu} = 0$, the critical condition gives $\Delta(0) = 1$, and the relation in (7) gives $\tau(0) = 1 + \frac{1}{r}$. Since $\tau^2(0) - 4\Delta(0) < 0$, the eigenvalues remain complex for sufficiently small $|\widetilde{\mu}|$ and satisfy

$$\lambda_{1,2}(\widetilde{\mu}) = \alpha(\widetilde{\mu}) \pm i\beta(\widetilde{\mu}) = \frac{\tau(\widetilde{\mu})}{2} \pm \frac{i}{2}\sqrt{4\Delta(\widetilde{\mu}) - \tau^2(\widetilde{\mu})}$$

In particular, $\lambda_{1,2}(0) = \alpha_0 \pm i\beta_0$, where

$$\alpha_0 = \alpha(0) = \frac{r+1}{2r}, \quad \beta_0 = \beta(0) = \frac{\sqrt{(r-1)(3r+1)}}{2r} > 0 \tag{11}$$

Since the eigenvalues' product equals the determinant, $|\lambda_{1,2}(\widetilde{\mu})| = \sqrt{\Delta(\widetilde{\mu})}$, so $|\lambda_{1,2}(0)| = 1$. The transversality condition is verified by differentiating the eigenvalue modulus at $\widetilde{\mu} = 0$, which gives

$$\frac{d|\lambda_{1,2}(\widetilde{\mu})|}{d\widetilde{\mu}}\Big|_{\widetilde{\mu}=0} = \frac{1}{2}\Delta'(0) = -\frac{r(r-1)\mu^*}{2(1-\mu^*)(1-r\mu^*)} < 0 \tag{12}$$

Thus, the transversality condition holds; in particular, the eigenvalues move outside the unit circle for $\mu < \mu^*$ sufficiently close to $\mu^*$. This loss of local stability indicates the occurrence of a local bifurcation, from which an invariant closed curve may arise.

The additional nonresonance requirement is the absence of strong resonance. From (11), it follows that $\frac{1}{2} < \alpha_0 < 1$ and $\beta_0 > 0$. Therefore, the critical eigenvalues cannot be roots of unity of order $1, 2, 3$, or $4$. Consequently, the nonresonance condition is verified as

$$(\lambda_{1,2}(0))^m \neq 1, \quad m = 1, 2, 3, 4 \tag{13}$$

The stability of the bifurcating invariant closed curve is determined through the normal-form coefficient [25]. For this purpose, the coexistence fixed point is shifted to the origin and the system is expanded near the critical value. At $\mu = \mu^*$, recall that $L^* = \ln\left(\frac{r(1-\mu^*)}{1-r\mu^*}\right)$. The critical coexistence fixed point is

$$E_1^* = (H^*, P^*) = \left(\frac{L^*}{kc(r-1)}, \frac{L^*}{c}\right) \tag{14}$$

Let $u_t = H_t - H^*$, $v_t = P_t - P^*$, and $Z_t = (u_t, v_t)^T$, so that $E_1^*$ is translated to the origin. Set $\varepsilon = 1 - r\mu^*$. The critical condition in (9) and the expression for $H^*$ in (14) give $cH^*\varepsilon = \frac{1}{kr}$ and $ckH^*\varepsilon = \frac{1}{r}$. At $\mu = \mu^*$, the third-order expansion of the shifted system about the origin gives

$$\begin{aligned} u_{t+1} &= a_{10}u_t + a_{01}v_t + a_{20}u_t^2 + a_{11}u_tv_t + a_{02}v_t^2 + a_{30}u_t^3 + a_{21}u_t^2v_t + a_{12}u_tv_t^2 + a_{03}v_t^3 + O(\|Z_t\|^4) \\ v_{t+1} &= b_{10}u_t + b_{01}v_t + b_{20}u_t^2 + b_{11}u_tv_t + b_{02}v_t^2 + b_{30}u_t^3 + b_{21}u_t^2v_t + b_{12}u_tv_t^2 + b_{03}v_t^3 + O(\|Z_t\|^4) \end{aligned} \tag{15}$$

In (15), the only nonzero coefficients are

$$\begin{aligned} &a_{10} = 1, \quad a_{01} = -\frac{1}{kr}, \quad a_{11} = -c\varepsilon, \quad a_{02} = \frac{c}{2kr}, \quad a_{12} = \frac{c^2\varepsilon}{2}, \quad a_{03} = -\frac{c^2}{6kr} \\ &b_{10} = k(r-1), \quad b_{01} = \frac{1}{r}, \quad b_{11} = kc\varepsilon, \quad b_{02} = -\frac{c}{2r}, \quad b_{12} = -\frac{kc^2\varepsilon}{2}, \quad b_{03} = \frac{c^2}{6r} \end{aligned}$$

The first-order terms in (15) form the linear part, while the higher-order terms form the nonlinear remainder. Hence, $Z_{t+1} = MZ_t + N(Z_t)$, where

$$M = \begin{pmatrix} a_{10} & a_{01} \\ b_{10} & b_{01} \end{pmatrix} = \begin{pmatrix} 1 & -\frac{1}{kr} \\ k(r-1) & \frac{1}{r} \end{pmatrix}, \qquad N(Z_t) = \begin{pmatrix} F(u_t, v_t) \\ G(u_t, v_t) \end{pmatrix}$$

where $F$ and $G$ denote the nonlinear terms in the respective components. Up to third order,

$$F(u_t, v_t) = -c\varepsilon u_t v_t + \frac{c}{2kr} v_t^2 + \frac{c^2\varepsilon}{2} u_t v_t^2 - \frac{c^2}{6kr} v_t^3 + O(\|Z_t\|^4)$$
$$G(u_t, v_t) = kc\varepsilon u_t v_t - \frac{c}{2r} v_t^2 - \frac{kc^2\varepsilon}{2} u_t v_t^2 + \frac{c^2}{6r} v_t^3 + O(\|Z_t\|^4)$$

The relation $G(u_t, v_t) = -kF(u_t, v_t)$ simplifies the transformation to normal form. The matrix $M$ has the critical complex-conjugate eigenvalues, where $\alpha_0$ and $\beta_0$ are given in (11). Since $a_{01} \neq 0$ and $\beta_0 > 0$, the standard real transformation may be used. Moreover, $\det(T) = -a_{01}\beta_0 = \beta_0/(kr) > 0$; thus, $T$ is invertible. The transformation matrix and its inverse are

$$T = \begin{pmatrix} a_{01} & 0 \\ \alpha_0 - a_{10} & -\beta_0 \end{pmatrix} = \begin{pmatrix} -\frac{1}{kr} & 0 \\ \frac{1-r}{2r} & -\beta_0 \end{pmatrix}, \qquad T^{-1} = \begin{pmatrix} -kr & 0 \\ -\frac{k(1-r)}{2\beta_0} & -\frac{1}{\beta_0} \end{pmatrix}$$

Introduce $W_t = (X_t, Y_t)^T$ and set $Z_t = TW_t$. Thus, $u_t = -\frac{1}{kr} X_t$ and $v_t = \frac{1-r}{2r} X_t - \beta_0 Y_t$. For the nonlinear part, substituting these coordinate expressions into $F(u_t, v_t)$ gives

$$F(TW_t) = f_{20}X_t^2 + f_{11}X_tY_t + f_{02}Y_t^2 + f_{30}X_t^3 + f_{21}X_t^2Y_t + f_{12}X_tY_t^2 + f_{03}Y_t^3 + O(\|W_t\|^4)$$

where

$$f_{20} = \frac{c\varepsilon(1-r)}{2kr^2} + \frac{c(1-r)^2}{8kr^3}, \quad f_{11} = -\frac{c\varepsilon\beta_0}{kr} - \frac{c(1-r)\beta_0}{2kr^2}, \quad f_{02} = \frac{c\beta_0^2}{2kr},$$
$$f_{30} = -\frac{c^2\varepsilon(1-r)^2}{8kr^3} - \frac{c^2(1-r)^3}{48kr^4}, \quad f_{21} = \frac{c^2\varepsilon(1-r)\beta_0}{2kr^2} + \frac{c^2(1-r)^2\beta_0}{8kr^3},$$
$$f_{12} = -\frac{c^2\varepsilon\beta_0^2}{2kr} - \frac{c^2(1-r)\beta_0^2}{4kr^2}, \quad f_{03} = \frac{c^2\beta_0^3}{6kr}$$

The relation $G(u_t, v_t) = -kF(u_t, v_t)$ holds for all $(u_t, v_t)$ near the origin. Evaluating it at $(u_t, v_t) = TW_t$ therefore gives $G(TW_t) = -kF(TW_t)$.

Substituting $Z_t = TW_t$ into $Z_{t+1} = MZ_t + N(Z_t)$ gives $TW_{t+1} = MTW_t + N(TW_t)$. Multiplication by $T^{-1}$ then yields $W_{t+1} = T^{-1}MTW_t + T^{-1}N(TW_t)$. Using the matrices above, direct multiplication puts the linear part into real rotational form. Moreover, using the relation between $F(TW_t)$ and $G(TW_t)$, the nonlinear vector becomes $N(TW_t) = (F(TW_t), -kF(TW_t))^T$. Applying $T^{-1}$ to the vector $N(TW_t)$ then gives

$$W_{t+1} = \begin{pmatrix} \alpha_0 & -\beta_0 \\ \beta_0 & \alpha_0 \end{pmatrix} W_t + \begin{pmatrix} -krF(TW_t) \\ \frac{k(r+1)}{2\beta_0} F(TW_t) \end{pmatrix}$$

Define $\mathcal{F}(X_t, Y_t) = -krF(TW_t)$ and $\mathcal{G}(X_t, Y_t) = \frac{k(r+1)}{2\beta_0} F(TW_t)$. The transformed system is therefore written componentwise as

$$X_{t+1} = \alpha_0 X_t - \beta_0 Y_t + \mathcal{F}(X_t, Y_t)$$
$$Y_{t+1} = \beta_0 X_t + \alpha_0 Y_t + \mathcal{G}(X_t, Y_t)$$

The transformed nonlinear components can be expressed as

$$\mathcal{F}(X_t, Y_t) = A_{20}X_t^2 + A_{11}X_tY_t + A_{02}Y_t^2 + A_{30}X_t^3 + A_{21}X_t^2Y_t + A_{12}X_tY_t^2 + A_{03}Y_t^3 + O(\|W_t\|^4)$$
$$\mathcal{G}(X_t, Y_t) = B_{20}X_t^2 + B_{11}X_tY_t + B_{02}Y_t^2 + B_{30}X_t^3 + B_{21}X_t^2Y_t + B_{12}X_tY_t^2 + B_{03}Y_t^3 + O(\|W_t\|^4)$$

The corresponding coefficients satisfy $A_{ij} = -krf_{ij}$ and $B_{ij} = \frac{k(r+1)}{2\beta_0} f_{ij}$. In particular, the coefficients of $\mathcal{F}$ are

$$A_{20} = -\frac{c\varepsilon(1-r)}{2r} - \frac{c(1-r)^2}{8r^2}, \quad A_{11} = c\varepsilon\beta_0 + \frac{c(1-r)\beta_0}{2r}, \quad A_{02} = -\frac{c\beta_0^2}{2}$$
$$A_{30} = \frac{c^2\varepsilon(1-r)^2}{8r^2} + \frac{c^2(1-r)^3}{48r^3}, \quad A_{21} = -\frac{c^2\varepsilon(1-r)\beta_0}{2r} - \frac{c^2(1-r)^2\beta_0}{8r^2}$$
$$A_{12} = \frac{c^2\varepsilon\beta_0^2}{2} + \frac{c^2(1-r)\beta_0^2}{4r}, \quad A_{03} = -\frac{c^2\beta_0^3}{6}$$

Meanwhile, the coefficients of $\mathcal{G}$ are

$$B_{20} = \frac{c(r+1)\varepsilon(1-r)}{4\beta_0 r^2} + \frac{c(r+1)(1-r)^2}{16\beta_0 r^3}, \quad B_{11} = -\frac{c(r+1)\varepsilon}{2r} - \frac{c(r+1)(1-r)}{4r^2}$$
$$B_{02} = \frac{c(r+1)\beta_0}{4r}, \quad B_{30} = -\frac{c^2(r+1)\varepsilon(1-r)^2}{16\beta_0 r^3} - \frac{c^2(r+1)(1-r)^3}{96\beta_0 r^4}$$
$$B_{21} = \frac{c^2(r+1)\varepsilon(1-r)}{4r^2} + \frac{c^2(r+1)(1-r)^2}{16r^3}$$
$$B_{12} = -\frac{c^2(r+1)\varepsilon\beta_0}{4r} - \frac{c^2(r+1)(1-r)\beta_0}{8r^2}, \quad B_{03} = \frac{c^2(r+1)\beta_0^2}{12r}$$

Therefore, at $\mu = \mu^*$, the shifted system is expressed in standard real rotational form, with its nonlinear terms represented by the coefficients $A_{ij}$ and $B_{ij}$. The required partial derivatives of the transformed nonlinear components at the origin are obtained directly from $\mathcal{F}(X_t, Y_t)$ and $\mathcal{G}(X_t, Y_t)$. All derivatives in this part are evaluated at the origin $(X, Y) = (0, 0)$. Thus,

$$\mathcal{F}_{XX} = 2A_{20}, \quad \mathcal{F}_{XY} = A_{11}, \quad \mathcal{F}_{YY} = 2A_{02},$$
$$\mathcal{F}_{XXX} = 6A_{30}, \quad \mathcal{F}_{XXY} = 2A_{21}, \quad \mathcal{F}_{XYY} = 2A_{12}, \quad \mathcal{F}_{YYY} = 6A_{03}$$

Similarly, the required derivatives of $\mathcal{G}$ are

$$\mathcal{G}_{XX} = 2B_{20}, \quad \mathcal{G}_{XY} = B_{11}, \quad \mathcal{G}_{YY} = 2B_{02},$$
$$\mathcal{G}_{XXX} = 6B_{30}, \quad \mathcal{G}_{XXY} = 2B_{21}, \quad \mathcal{G}_{XYY} = 2B_{12}, \quad \mathcal{G}_{YYY} = 6B_{03}$$

To determine the stability of the invariant closed curve bifurcating from the Neimark–Sacker bifurcation, the normal-form coefficient is computed following Guckenheimer and Holmes [25]. Let $\lambda_1 = \alpha_0 + i\beta_0$ and $\lambda_2 = \alpha_0 - i\beta_0$. The determining coefficient is given by

$$\Omega = -\operatorname{Re}\left[\frac{(1-2\lambda_1)\lambda_2^2}{1-\lambda_1}\xi_{11}\xi_{20}\right] - \frac{1}{2}|\xi_{11}|^2 - |\xi_{02}|^2 + \operatorname{Re}(\lambda_2\xi_{21}) \tag{16}$$

where

$$\xi_{20} = \frac{1}{8}\left[(\mathcal{F}_{XX} - \mathcal{F}_{YY} + 2\mathcal{G}_{XY}) + i(\mathcal{G}_{XX} - \mathcal{G}_{YY} - 2\mathcal{F}_{XY})\right]$$
$$\xi_{11} = \frac{1}{4}\left[(\mathcal{F}_{XX} + \mathcal{F}_{YY}) + i(\mathcal{G}_{XX} + \mathcal{G}_{YY})\right]$$
$$\xi_{02} = \frac{1}{8}\left[(\mathcal{F}_{XX} - \mathcal{F}_{YY} - 2\mathcal{G}_{XY}) + i(\mathcal{G}_{XX} - \mathcal{G}_{YY} + 2\mathcal{F}_{XY})\right]$$
$$\xi_{21} = \frac{1}{16}\left[(\mathcal{F}_{XXX} + \mathcal{F}_{XYY} + \mathcal{G}_{XXY} + \mathcal{G}_{YYY}) + i(\mathcal{G}_{XXX} + \mathcal{G}_{XYY} - \mathcal{F}_{XXY} - \mathcal{F}_{YYY})\right]$$

Using the partial derivatives above, straightforward computation yields

$$\xi_{20} = -\frac{c\left(4r\varepsilon - r + 1 + 2ir\beta_0\right)\left(4r\beta_0 + i(4r^2\beta_0^2 + r^2 - 1)\right)}{64r^3\beta_0}$$
$$\xi_{11} = \frac{c\left(i(r+1) - 2r\beta_0\right)\left(4r^2\beta_0^2 + 4r\varepsilon(1-r) + (r-1)^2\right)}{32r^3\beta_0}$$
$$\xi_{02} = -\frac{c\left(4r^2\beta_0 + i(4r^2\beta_0^2 - r^2 + 1)\right)\left(r - 4r\varepsilon - 1 + 2ir\beta_0\right)}{64r^3\beta_0}$$
$$\xi_{21} = \frac{c^2\left(4r\beta_0 + i(4r^2\beta_0^2 + r^2 - 1)\right)\left(4r^2\beta_0^2 + (r-1)^2 + 6r\varepsilon(1-r) - 4ir^2\beta_0\varepsilon\right)}{256r^4\beta_0}$$

Substituting these coefficients into (16) gives

$$\Omega = -\frac{c^2}{16r}\left(r + \varepsilon - 2r\varepsilon + 2r\varepsilon^2 - 1\right) \tag{17}$$

Let $P_\Omega = r + \varepsilon - 2r\varepsilon + 2r\varepsilon^2 - 1$; then $\Omega = -c^2 P_\Omega/(16r)$. Since $c > 0$ and $r > 1$, the sign of $\Omega$ is opposite to that of $P_\Omega$. From $\varepsilon = 1 - r\mu^*$, one obtains $\mu^* = (1-\varepsilon)/r$. Substitution into the critical condition (9) gives $\varepsilon \ln\left(\frac{r-1+\varepsilon}{\varepsilon}\right) = \frac{r-1}{r}$. Now set $s = (r-1)/\varepsilon$ and $h = \ln(1+s)$. Then $s, h > 0$, and this equation yields

$$r = \frac{s}{h}, \qquad \varepsilon = \frac{s-h}{sh}, \qquad P_\Omega = \frac{(s-h)K}{sh^3}$$

where $K = sh^2 - 2sh + 2s + h^2 - 2h$. Since $s = e^h - 1$ and $h > 0$, the Maclaurin expansion gives $e^h > 1 + h + \frac{h^2}{2}$; hence, $s - h > 0$. Moreover, $h^2 - 2h + 2 = (h-1)^2 + 1 > 0$, and the same inequality gives

$$\begin{aligned} K &= e^h(h^2 - 2h + 2) - 2 \\ &> \left(1 + h + \frac{h^2}{2}\right)(h^2 - 2h + 2) - 2 = \frac{h^4}{2} > 0 \end{aligned}$$

Since $P_\Omega > 0$, the nondegeneracy condition $\Omega \neq 0$ follows from

$$\Omega < 0 \tag{18}$$

The preceding results verify the unit-circle crossing, transversality, nonresonance, and normal-form nondegeneracy conditions. These results are summarized in the following theorem.

**Theorem 7.** *Assume that $(r, k, c, \mu^*) \in \mathcal{H}_{\mathrm{NS}}$ in (10). Then system (1) undergoes a Neimark–Sacker bifurcation at the critical coexistence fixed point $E_1^* = (H^*, P^*)$ in (14) as $\mu$ varies through $\mu^*$. Since $\Omega < 0$, the bifurcation is supercritical. Consequently, a stable invariant closed curve bifurcates from $E_1^*$ for $\mu < \mu^*$ sufficiently close to $\mu^*$.*

*Proof.* By Theorem 6, at $\mu = \mu^*$, the eigenvalues of the Jacobian matrix at $E_1^*$ are complex conjugates and lie on the unit circle. The transversality condition follows from (12), while the nonresonance condition is verified in (13). Furthermore, the normal-form coefficient satisfies $\Omega < 0$ by (18). Hence, the Neimark–Sacker bifurcation is supercritical and the bifurcating invariant closed curve is stable. Based on Theorem 4, the coexistence fixed point $E_1$ is locally asymptotically stable whenever $\Delta < 1$. As $\mu$ decreases through $\mu^*$, the transversality condition shows that $E_1$ loses its stability. Since $\Omega < 0$, a stable invariant closed curve bifurcates for $\mu < \mu^*$ sufficiently close to $\mu^*$. Therefore, the system undergoes a supercritical Neimark–Sacker bifurcation at $\mu = \mu^*$. □

### 3.5. Numerical Simulations

The numerical simulations presented below corroborate and illustrate the analytical results obtained previously. All numerical computations were performed using MATLAB. Figures 1, 2, and 3 were generated by direct iteration of system (1), whereas Figure 4 was constructed by numerically evaluating the analytical existence and local-stability conditions over the $(r, \mu)$ parameter plane. Unless otherwise stated, $k = 1$ and $c = 1$ are used as reference parameter values. Under the rescaling $H_t^{\mathrm{sc}} = kcH_t$ and $P_t^{\mathrm{sc}} = cP_t$, the system becomes independent of $k$ and $c$, showing that these parameters affect the population scales but not the qualitative dynamics determined by $r$ and $\mu$. In particular, the local-stability conditions, the node–spiral classification, and the critical Neimark–Sacker condition $\Delta = 1$ are independent of $k$ and $c$, while the sign of the normal-form coefficient $\Omega$ is also unaffected by these parameters.

The parameter choices also have a biological interpretation. The values $r = 0.95$, 1, 1.5, and 2 represent host reproduction below, at, and above the replacement threshold, while $\mu$ denotes the protected host fraction and its selected values represent different levels of protection, including the

transition near $\mu^*$. Habib et al. [12] reported an overall negative relationship between the depth of *Bactrocera dorsalis* pupae in plant debris and parasitism by *Dirhinus giffardii*, illustrating how spatial concealment can reduce parasitoid access. This comparison is qualitative; the selected values are not species-specific estimates.

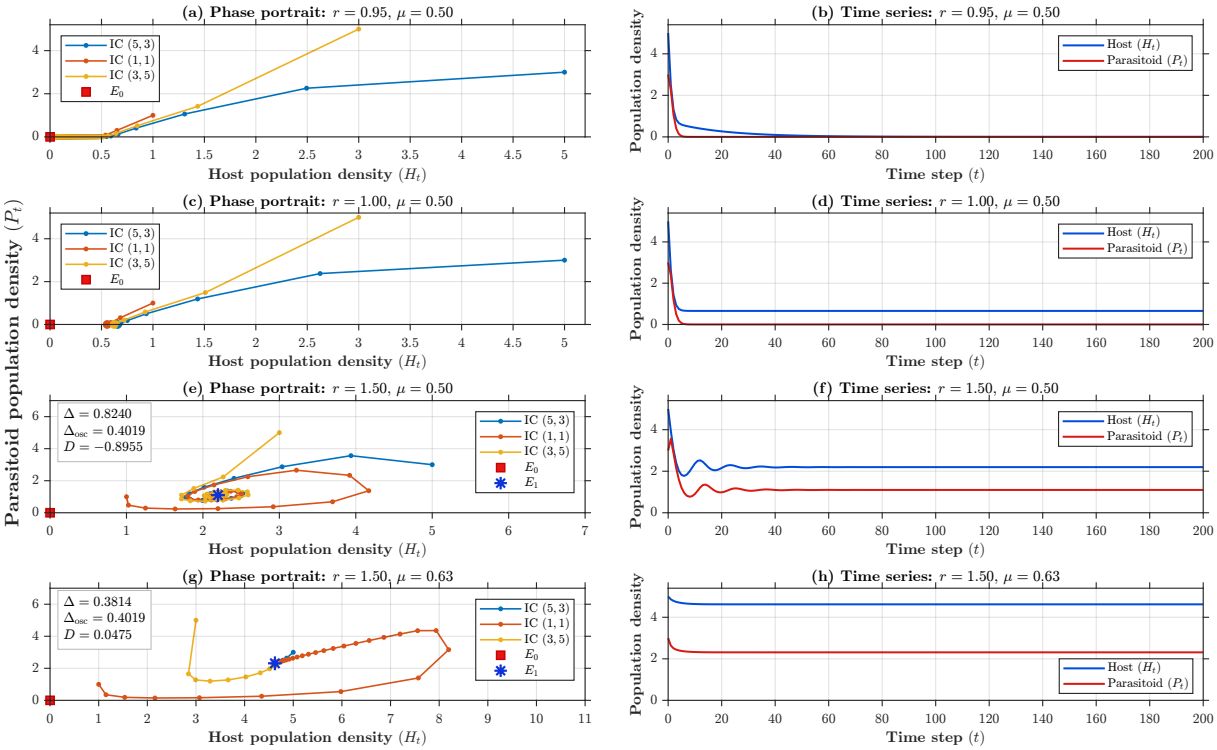


**Fig. 1:** Panels (a)–(b) show stable extinction, panels (c)–(d) show the threshold with a continuum of boundary fixed points, panels (e)–(f) show spiral convergence, and panels (g)–(h) show node-type convergence. IC denotes the initial condition.

For Figure 1, system (1) was directly iterated with four parameter cases: $(r, \mu) = (0.95, 0.50)$, $(1.00, 0.50)$, $(1.50, 0.50)$, and $(1.50, 0.63)$. The first two cases kept $\mu = 0.50$ fixed while varying $r$, whereas the last two kept $r = 1.50$ fixed while varying $\mu$. Each phase portrait was generated from $(H_0, P_0) = (5, 3)$, $(1, 1)$, and $(3, 5)$, while the corresponding time series used $(H_0, P_0) = (5, 3)$. Each orbit was iterated over $t = 0, \ldots, 200$ without transient removal. The logarithmic quantity $L$ and the coexistence fixed point $E_1$, when it exists, were evaluated from Proposition 1, while $\Delta$, $\Delta_{\text{osc}}$, and $D$ shown in the coexistence panels were computed from (6), (8), and (3), respectively.

The resulting trajectories are consistent with the local fixed-point results obtained analytically. In panels (a)–(b), both populations approach extinction, in agreement with Theorem 3. Panels (c)–(d) illustrate the threshold $r = 1$, where the parasitoid population tends to zero while the limiting host density depends on the initial condition, consistent with the continuum of boundary fixed points in Section 3.3. For the coexistence cases, panels (e)–(f) show damped oscillatory convergence to $E_1$, corresponding to the spiral-sink behavior established in Theorems 4 and 5, whereas panels (g)–(h) show node-type convergence. These coexistence patterns are consistent with the node–spiral classification determined by the threshold $\Delta_{\text{osc}}$ in (8).

For Figure 2, $r = 2$ is fixed and the determinant $\Delta(\mu)$ was evaluated from (6). The critical refuge value was computed as the root of $\Delta(\mu) - 1 = 0$ using the MATLAB `fzero` routine on the bracket $\left[10^{-10}, \frac{1}{r} - 10^{-10}\right]$, giving $\mu^* \approx 0.3010237263$. A descending grid of 800 equally spaced refuge values from $\mu = 0.499$ to $\mu = 0.20$ was generated using `linspace`. Starting from $(H_0, P_0) = (1, 1)$, system (1) was directly iterated sequentially over this grid, with the final state at each refuge value used as the initial condition for the next. For each value of $\mu$, the first $24,000$ iterations were discarded as transients and the subsequent 300 states were retained. For $\mu > \mu^*$,

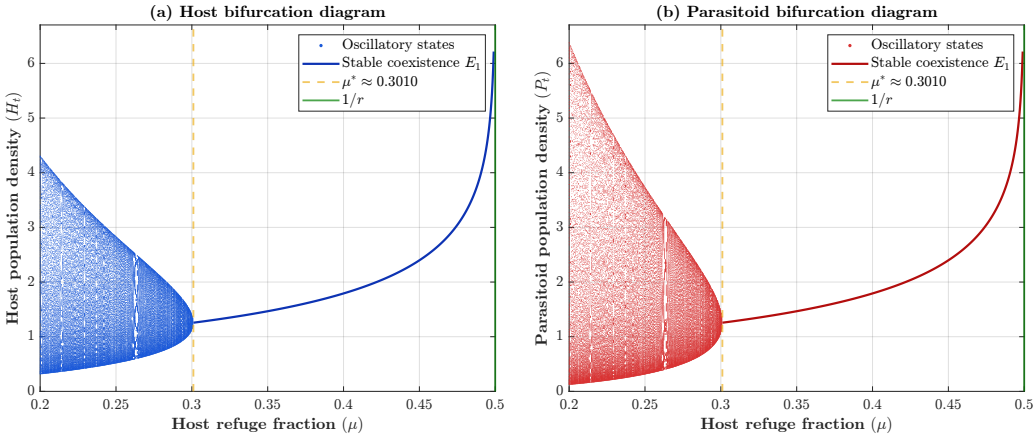


**Fig. 2:** Host and parasitoid bifurcation diagrams for $r = 2$.

the mean of the retained states was used to represent the stable-coexistence branch, whereas for $\mu < \mu^*$, the retained states were used to represent the post-bifurcation oscillatory behavior.

The resulting diagram is consistent with the local stability and bifurcation results established analytically. For $\mu^* < \mu < \frac{1}{r}$, the retained states converge to a single density pair corresponding to the locally asymptotically stable coexistence fixed point $E_1$, in agreement with Theorem 4. As $\mu$ decreases through $\mu^*$, $E_1$ loses local stability when $\Delta(\mu^*) = 1$. On the weak-refuge side, for $\mu < \mu^*$ sufficiently close to $\mu^*$, the retained states form persistent oscillatory bands around $E_1$, consistent with the stable invariant closed curve generated by the supercritical Neimark–Sacker bifurcation established in Theorem 7.

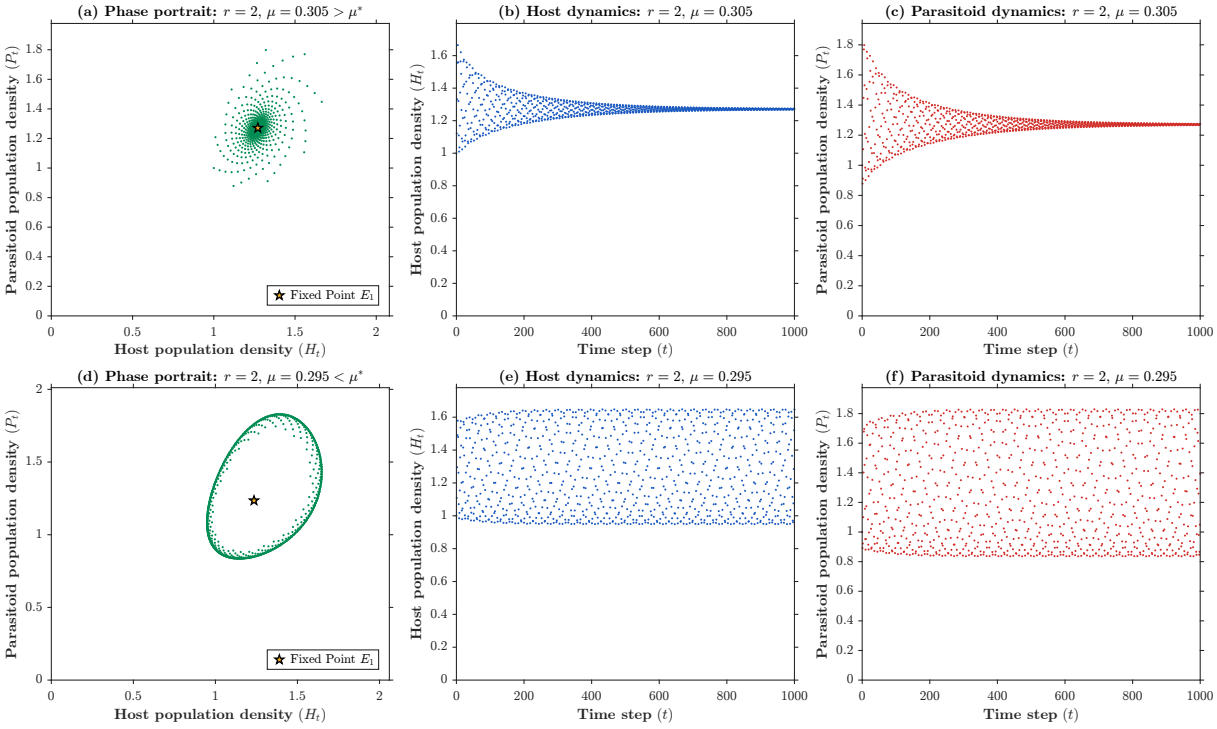


**Fig. 3:** Panels (a)–(c) show damped convergence toward the coexistence fixed point, whereas panels (d)–(f) show sustained bounded oscillations around the unstable coexistence fixed point.

For Figure 3, $r = 2$ and the critical refuge value was obtained by solving $\Delta(\mu) - 1 = 0$, with $\Delta(\mu)$ evaluated from (6), using the MATLAB `fzero` routine on the bracket $\left[10^{-10}, \frac{1}{r} - 10^{-10}\right]$. This calculation gave $\mu^* \approx 0.3010237263$, and two refuge values were selected: $\mu = 0.305$ and $\mu = 0.295$. For each value, system (1) was initialized independently at $(H_0, P_0) = (1, 1)$ and

directly iterated over $t = 0, \ldots, 1000$ without transient removal. The coexistence fixed point $E_1$ shown in each phase portrait was evaluated from Proposition 1.

The numerical results illustrate the local dynamical transition established analytically. For $\mu = 0.305 > \mu^*$, panels (a)–(c) show trajectories spiraling toward $E_1$, with oscillations of progressively decreasing amplitude, consistent with the local asymptotic stability condition in Theorem 4. For $\mu = 0.295 < \mu^*$, panels (d)–(f) show that the trajectory is no longer attracted to $E_1$ but approaches a closed curve surrounding it, while the host and parasitoid populations exhibit sustained bounded oscillations. Since this refuge value lies on the weak-refuge side sufficiently close to $\mu^*$, the observed behavior is consistent with the stable invariant closed curve established locally by the supercritical Neimark–Sacker bifurcation in Theorem 7.

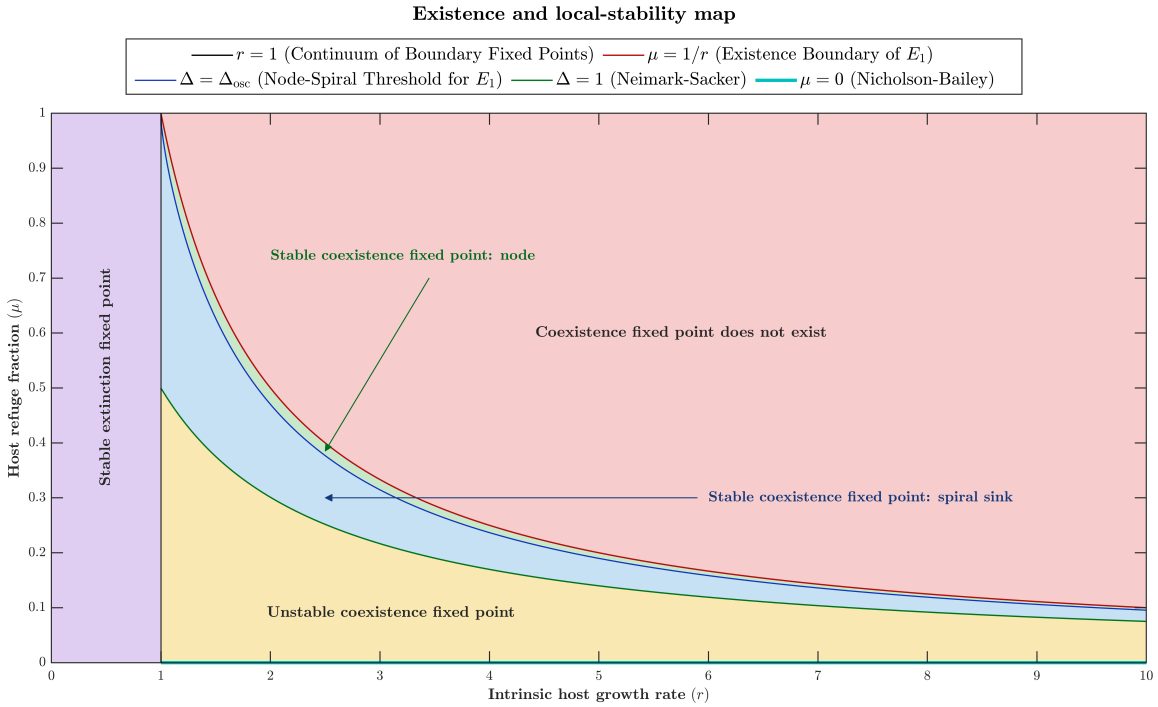


**Fig. 4:** Existence and local-stability map in the $(r, \mu)$ parameter plane.

Figure 4 was constructed from $1,200$ equally spaced values over $0.001 \leq r \leq 10$ and 800 equally spaced values over $0 \leq \mu \leq 1 - 10^{-6}$, generated using `linspace` and combined into a rectangular parameter grid using `meshgrid`. Grid points with $r < 1$ were assigned to the stable-extinction region, while those with $r > 1$ and $\mu > \frac{1}{r}$ were assigned to the region where $E_1$ does not exist. For $r > 1$ and $0 < \mu < \frac{1}{r}$, $L$ was evaluated from Proposition 1, $\Delta$ from (6), and $\Delta_{\text{osc}}$ from (8); the points were then classified as stable nodes when $0 < \Delta < \Delta_{\text{osc}}$, spiral sinks when $\Delta_{\text{osc}} < \Delta < 1$, and unstable coexistence fixed points when $\Delta > 1$. The explicit boundaries $r = 1$ and $\mu = \frac{1}{r}$, together with the segment $\mu = 0$ for $1 \leq r \leq 10$, were plotted directly, whereas the implicit boundary curves $\Delta = \Delta_{\text{osc}}$ and $\Delta = 1$ were traced from the computed grid using the MATLAB `contour` routine. Because the map was obtained by evaluating analytical expressions rather than by iterating system (1), no transient processing was required.

The map first separates the parameter regions according to fixed-point existence. For $0 < r < 1$, the extinction fixed point $E_0$ is locally asymptotically stable, as established in Theorem 3. The line $r = 1$ marks the nonhyperbolic extinction threshold at which the model admits the continuum of boundary fixed points $\{(\bar{H}, 0) \mid \bar{H} \geq 0\}$ described in Section 3.3. For $r > 1$, the coexistence fixed point $E_1$ exists only when $0 \leq \mu < \frac{1}{r}$, and the curve $\mu = \frac{1}{r}$ therefore forms its existence boundary. Above this boundary, $E_1$ does not exist, although the extinction fixed point $E_0$ continues to exist and is unstable. Accordingly, the region above $\mu = \frac{1}{r}$ indicates only that the coexistence fixed point $E_1$ does not exist and does not provide a classification of

the resulting trajectories.

Within the existence region $r > 1$ and $0 < \mu < \frac{1}{r}$, the map displays the local classifications of $E_1$ determined by Theorems 4 and 5. The region $0 < \Delta < \Delta_{\text{osc}}$ corresponds to a stable coexistence fixed point of node type, the curve $\Delta = \Delta_{\text{osc}}$ marks the repeated-real-eigenvalue threshold, and the region $\Delta_{\text{osc}} < \Delta < 1$ corresponds to a stable coexistence fixed point of spiral-sink type. At $\Delta = 1$, the complex-conjugate eigenvalues reach the unit circle, defining the Neimark–Sacker boundary established in Theorem 7. The region $\Delta > 1$ corresponds analytically to an unstable coexistence fixed point $E_1$. For $\mu < \mu^*$ sufficiently close to $\mu^*$, Theorem 7 further establishes the existence of a stable invariant closed curve surrounding $E_1$. The line $\mu = 0$ is displayed separately as the Nicholson–Bailey boundary, where the refuge mechanism is absent and $E_1$ is unstable for $r > 1$.

### 3.6. Discussion

The results obtained in this study show that a Neimark–Sacker transition can also occur when intrinsic host self-limitation is absent. This complements the analysis of Bešo et al. [18], which established Neimark–Sacker bifurcation for refuge models with Beverton–Holt host growth and a general escape response. Thus, although the two formulations use different assumptions, both demonstrate that variation in host protection can change the local stability of coexistence.

The present analysis adopts the proportional-refuge formulation considered by Singh [21], specifically the case without intrinsic host self-limitation. Singh examined this case within a broader investigation of the limits of parasitoid-driven host suppression and its implications for biological control, identifying the coexistence stability boundary and reporting bounded oscillations under weak refuge. The present study focuses on the local dynamical structure of the same formulation. Theorem 5 distinguishes non-oscillatory node-type convergence from damped spiral convergence within the stable region, while Section 3.3 characterizes the continuum of boundary fixed points at $r = 1$. As a supporting result, Proposition 2 establishes the existence and uniqueness of $\mu^*$ in the admissible interval for every $r > 1$, providing the critical value used in the main bifurcation theorem. Theorem 7 then verifies the unit-circle condition, transversality, nonresonance, and normal-form nondegeneracy conditions, proves that $\Omega < 0$, and establishes a supercritical Neimark–Sacker bifurcation with a stable invariant closed curve arising for $\mu < \mu^*$ sufficiently close to $\mu^*$.

These local analytical results are organized in the $(r, \mu)$ parameter map in Figure 4. The map combines the fixed-point existence boundaries with the node–spiral and Neimark–Sacker thresholds, thereby organizing the locally stable extinction region together with the existence and local-stability classifications of the coexistence fixed point. Its scope is limited to fixed-point existence and local stability rather than a global classification of all possible trajectories, while the stable invariant closed curve is established only for $\mu < \mu^*$ sufficiently close to the Neimark–Sacker threshold.

## 4. Conclusion

This study examined the local dynamics of a discrete-time host–parasitoid model with a proportional refuge mechanism. The extinction fixed point is locally asymptotically stable for low intrinsic host growth, whereas the boundary between extinction and coexistence is a nonhyperbolic threshold at which the model admits a continuum of boundary fixed points. For the coexistence fixed point, an explicit local-stability condition was obtained, and the stable regime was further separated into node-type and spiral-sink convergence by a discriminant threshold.

Variation in the refuge fraction can produce a supercritical Neimark–Sacker bifurcation: as the coexistence fixed point loses local stability, a stable invariant closed curve arises on the weak-refuge side sufficiently close to the critical threshold. The numerical simulations corroborate the fixed-point classifications and the local bifurcation behavior, while the $(r, \mu)$ map organizes the fixed-point existence and local-stability regions and displays the boundaries $r = 1$, $\mu = \frac{1}{r}$,

$\Delta = \Delta_{\mathrm{osc}}$, and $\Delta = 1$. Thus, the analysis complements the existing regime description by clarifying the local transitions within the refuge model. In the refuge-free limit, the model recovers Nicholson–Bailey-type boom-and-bust dynamics.

## CRediT Authorship Contribution Statement

**Ardianto Ramadhan:** Methodology, Model Analysis, Visualization, Writing–Original Draft Preparation. **Abadi:** Supervision, Validation, Writing–Review & Editing.

## Declaration of Generative AI and AI-assisted technologies

During manuscript preparation, the authors used ChatGPT (OpenAI) for language refinement, including grammar, clarity, and readability. All AI-assisted suggestions were reviewed and revised by the authors to ensure the accuracy and integrity of the final manuscript.

## Declaration of Competing Interest

The authors declare no competing interests.

## Funding and Acknowledgments

This research received no external funding.

## Data and Code Availability

No external datasets were used in this study. The MATLAB simulation codes and Wolfram Language files used for the normal-form verification are provided as supplementary materials.

## References

[1] Y. Difaa, B. Khajji, and H. Benaissa. “Discrete Mathematical Model of Fast Food Consumption: Control Approach”. In: *Communication in Biomathematical Sciences* 8.1 (2025), pp. 66–78. DOI: 10.5614/cbms.2025.8.1.5.

[2] M. Li, N. Xie, R. Zhang, and X. Huang. “Dynamics of a Discrete Lotka–Volterra Information Diffusion Model”. In: *International Journal of Bifurcation and Chaos* 32.15 (2022), p. 2250228. DOI: 10.1142/S0218127422502285.

[3] P. A. Naik, Z. Eskandari, Z. Avazzadeh, and J. Zu. “Multiple Bifurcations of a Discrete-Time Prey–Predator Model with Mixed Functional Response”. In: *International Journal of Bifurcation and Chaos* 32.4 (2022), p. 2250050. DOI: 10.1142/S021812742250050X.

[4] D. Mukherjee. “Dynamics of a Discrete-Time Ecogenetic Predator–Prey Model”. In: *Communication in Biomathematical Sciences* 5.2 (2022), pp. 161–169. DOI: 10.5614/cbms.2022.5.2.5.

[5] S. H. Streipert, G. S. K. Wolkowicz, and M. Bohner. “Derivation and Analysis of a Discrete Predator–Prey Model”. In: *Bulletin of Mathematical Biology* 84.7 (2022), p. 67. DOI: 10.1007/s11538-022-01016-4.

[6] A. J. Nicholson and V. A. Bailey. “The Balance of Animal Populations—Part I”. In: *Proceedings of the Zoological Society of London* 105.3 (1935), pp. 551–598. DOI: 10.1111/j.1096-3642.1935.tb01680.x.

[7] X. Liu and Y. Liu. “Stability and Bifurcation Analysis of a Discrete-Time Host–Parasitoid Model with Holling III Functional Response”. In: *AIMS Mathematics* 8.10 (2023), pp. 22675–22692. DOI: 10.3934/math.20231154.

[8] S. Kalabušić and E. Pilav. "The Behavior of a Host–Parasitoid Model with Host Logistic Growth and Proportional Refuge". In: *International Journal of Biomathematics* 17.5 (2024), p. 2350043. DOI: 10.1142/S1793524523500432.

[9] Y. Liu, X. Liu, and L. Guo. "Complex Dynamics and Bifurcations in a Discrete Switching Host–Parasitoid Model Under a Nonlinear Threshold Policy". In: *Computation* 14.6 (2026), p. 133. DOI: 10.3390/computation14060133.

[10] B. Külahçıoğlu, Ü. Ufuktepe, and A. Kalampakas. "A Host–Parasitoid Dynamics with Allee and Refuge Effects". In: *European Journal of Pure and Applied Mathematics* 16.2 (2023), pp. 736–750. DOI: 10.29020/nybg.ejpam.v16i2.4707.

[11] E. Bešo, S. Kalabušić, and E. Pilav. "A General Egg-Limited and Search-Limited Host–Parasitoid Model with Proportional Host Refuge". In: *Applicable Analysis* 104.5 (2025), pp. 945–979. DOI: 10.1080/00036811.2024.2426082.

[12] Z. Habib, M. Ibrahim, N. Shah, I. Ullah, and N. J. Gill. "Effect of Host Pupae Age and Depth in Plant Debris on the Searching Efficiency of Pupal Parasitoid *Dirhinus giffardii* (Silvestri) on Oriental Fruit Fly *Bactrocera dorsalis* (Hendel)". In: *Sarhad Journal of Agriculture* 38.5 (2022), pp. 87–94. DOI: 10.17582/journal.sja/2022/38.5.87.94.

[13] X. Hu and S. R.-J. Jang. "The Role of Host Refuge and Strong Allee Effects in a Host–Parasitoid System". In: *International Journal of Biomathematics* 16.5 (2023), p. 2250107. DOI: 10.1142/S1793524522501078.

[14] M. S. Shabbir, Q. Din, W. F. Alfwzan, and M. De la Sen. "The Qualitative Analysis of Host–Parasitoid Model with Inclusion of Spatial Refuge Effect". In: *Axioms* 12.3 (2023), p. 290. DOI: 10.3390/axioms12030290.

[15] N. A. Hadinata, A. Suryanto, and W. M. Kusumawinahyu. "Bifurcation Analysis of a Discrete Logistic System with Additive Allee Effect and Feedback Control". In: *CAUCHY: Jurnal Matematika Murni dan Aplikasi* 9.2 (2024), pp. 199–211. DOI: 10.18860/ca.v9i2.26674.

[16] B. Hong and C. Zhang. "Neimark–Sacker Bifurcation of a Discrete-Time Predator–Prey Model with Prey Refuge Effect". In: *Mathematics* 11.6 (2023), p. 1399. DOI: 10.3390/math11061399.

[17] A. Q. Khan. "Neimark–Sacker Bifurcation of a Two-Dimensional Discrete-Time Predator–Prey Model". In: *SpringerPlus* 5 (2016), p. 126. DOI: 10.1186/s40064-015-1618-y.

[18] E. Bešo, S. Kalabušić, N. Mujić, and E. Pilav. "Neimark–Sacker Bifurcation and Stability of a Certain Class of Host–Parasitoid Models with Host Refuge Effect". In: *International Journal of Bifurcation and Chaos* 29.12 (2019), p. 1950169. DOI: 10.1142/S0218127419501694.

[19] Z. Ba and X. Li. "Period-Doubling Bifurcation and Neimark–Sacker Bifurcation of a Discrete Predator–Prey Model with Allee Effect and Cannibalism". In: *Electronic Research Archive* 31.3 (2023), pp. 1405–1438. DOI: 10.3934/era.2023072.

[20] S. Shoyimardonov. "Neimark–Sacker Bifurcation and Stability Analysis in a Discrete Phytoplankton–Zooplankton System with Holling Type II Functional Response". In: *Journal of Applied Analysis & Computation* 13.4 (2023), pp. 2048–2064. DOI: 10.11948/20220345.

[21] A. Singh. "Fundamental Limits of Parasitoid-Driven Host Population Suppression: Implications for Biological Control". In: *PLOS ONE* 18.12 (2023), e0295980. DOI: 10.1371/journal.pone.0295980.

[22] O. Galor. *Discrete Dynamical Systems*. Berlin, Heidelberg: Springer-Verlag, 2007. DOI: 10.1007/3-540-36776-4.

[23] S. N. Elaydi. *Discrete Chaos: With Applications in Science and Engineering*. 2nd ed. Boca Raton: Chapman and Hall/CRC, 2007. DOI: 10.1201/9781420011043.

[24] Y. A. Kuznetsov. *Elements of Applied Bifurcation Theory*. 2nd ed. New York: Springer-Verlag, 1998. DOI: 10.1007/b98848.

[25] J. Guckenheimer and P. Holmes. *Nonlinear Oscillations, Dynamical Systems, and Bifurcations of Vector Fields*. New York: Springer-Verlag, 1983. DOI: 10.1007/978-1-4612-1140-2.